

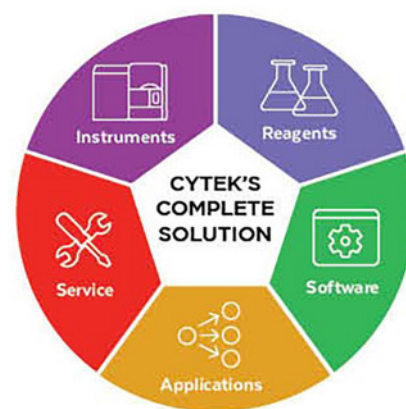
THE BEAUTY OF EXPRESSION

GIVE YOUR CELLS A VOICE



Your cells have a lot to say. Help them express themselves with high-quality single cell data thanks to Cytek's Full Spectrum Profiling™ (FSP™) technology and optimized flow cytometry applications.

- **Streamline** your workflow with highly sensitive, flexible instruments that eliminate the need to reconfigure for every assay
- **Accelerate** discovery with pre-optimized, ready-to-use reagent kits integrated with analysis templates
- **Maximize** efficiency with panel design tools and software that are widget-based and seamless
- **Partner** with highly trained service and application specialists that are ready to assist you with training and support

Cytek is committed to providing powerful solutions through scientific innovation. Join the world's most renowned pharmaceutical companies, CRO firms, industrial facilities, and research and academic institutions who have achieved results with our comprehensive approach. **Reveal the Beauty of Cellular Expression.**



Multi-omic and spatial dissection of immunotherapy response groups in non-small cell lung cancer

James Monkman¹  | Honesty Kim² | Aaron Mayer² | Ahmed Mehdi³ | Nicholas Matigian³ | Marie Cumberbatch⁴ | Milan Bhagat⁴ | Rahul Ladwa⁵ | Scott N. Mueller⁶ | Mark N. Adams⁷ | Ken O'Byrne^{5,7} | Arutha Kulasinghe¹ 

¹Frazer Institute, Faculty of Medicine, The University of Queensland, Woolloongabba, Brisbane, Queensland 4102, Australia

²Enable Medicine, Menlo Park, California, USA

³QFAB Bioinformatics, The University of Queensland, Brisbane, Queensland, Australia

⁴Tristar Technologies Group, Rockville, Maryland, USA

⁵Princess Alexandra Hospital, Brisbane, Queensland, Australia

⁶Department of Microbiology and Immunology, The University of Melbourne, at the Peter Doherty Institute for Infection and Immunity, Melbourne, Victoria, Australia

⁷Queensland University of Technology, Centre for Genomics and Personalised Health, School of Biomedical Sciences, Brisbane, Queensland, Australia

Correspondence

Ken O'Byrne: Queensland University of Technology, 37 Kent Street, Woolloongabba, QLD 4102, Australia.
Email: k.obyrne@qut.edu.au

Arutha Kulasinghe, Frazer Institute, Faculty of Medicine, The University of Queensland, 37 Kent Street, Woolloongabba, QLD 4102, Australia.
Email: arutha.kulasinghe@uq.edu.au

Funding information

Cure Cancer Australia Foundation, Grant/Award Number: 1182179; International Association for the Study of Lung Cancer; National Health and Medical Research Council, Grant/Award Number: 1157741; PA Research Foundation; International Association for the Study of Lung Cancer Foundation (IASLC)

Abstract

The composition and activation status of the cellular milieu contained within the tumour microenvironment (TME) is becoming increasingly recognized as a driving factor for immunotherapy response. Here, we employed multiplex immunohistochemistry (mIHC), and digital spatial profiling (DSP) to capture the targeted immune proteome and transcriptome of tumour and TME compartments from an immune checkpoint inhibitor (ICI)-treated ($n = 41$) non-small cell lung cancer (NSCLC) patient cohort. We demonstrate by mIHC that the interaction of CD68⁺ macrophages with PD1⁺, FoxP3⁺ cells is enriched in ICI refractory tumours ($p = 0.012$). Patients responsive to ICI therapy expressed higher levels of IL2 receptor alpha (CD25, $p = 0.028$) within their tumour compartments, which corresponded with increased *IL2* mRNA ($p = 0.001$) within their stroma. In addition, stromal *IL2* mRNA levels positively correlated with the expression of pro-apoptotic markers cleaved caspase 9 ($p = 2e^{-5}$) and BAD ($p = 5.5e^{-4}$) and negatively with levels of memory marker, CD45RO ($p = 7e^{-4}$). Immuno-inhibitory markers CTLA-4 ($p = 0.021$) and IDO-1 ($p = 0.023$) were suppressed in ICI-responsive patients. Tumour expression of CD44 was depleted in the responsive patients ($p = 0.02$), while higher stromal expression of one of its ligands, *SPP1* ($p = 0.008$), was observed. Cox survival analysis also indicated tumour CD44 expression was associated with poorer prognosis (hazard ratio [HR] = 1.61,

This is an open access article under the terms of the [Creative Commons Attribution](https://creativecommons.org/licenses/by/4.0/) License, which permits use, distribution and reproduction in any medium, provided the original work is properly cited.

© 2023 The Authors. *Immunology* published by John Wiley & Sons Ltd.

$p = 0.01$), consistent with its depletion in ICI-responsive patients. Through multi-modal approaches, we have dissected the characteristics of NSCLC immunotherapy treatment groups and provide evidence for the role of several markers including *IL2*, *CD25*, *CD44* and *SPP1* in the efficacy of current generations of ICI therapy.

KEYWORDS

immunotherapy, lung cancer, multi-omic, multiplex, spatial transcriptomics

INTRODUCTION

Lung cancer is the leading cause of cancer-related mortality in men and second cause of cancer mortality in women, with 5-year overall survival (OS) rates between 10% and 20% [1]. Of these cases, long-term benefits to PD-1/PD-L1 immune checkpoint inhibitors (ICIs) are observed in less than 30%. Thus, there is currently an unmet clinical need for predictive biomarkers for ICI therapy to better stratify patients for treatment [2–4]. Both tumour cell expression of PD-L1 [5] and tumour mutation burden (TMB) [6, 7] are FDA-approved companion diagnostic biomarker tests used to stratify patients for immunotherapy; however, these appear to be independent variables in their predictive capacity [6, 8, 9]. Difficulties in the implementation and assessment of these assays suggest that much remains to be discovered to understand the biological cues that dictate ICI response.

Therapy response and tumour progression are governed by tumour intrinsic features and their inherit interaction with the cellular composition of the tumour microenvironment (TME) [10]. Such interactions activate or suppress inflammatory signalling and immune cell recruitment, disrupt antigen presentation, remodel the extracellular matrix (ECM), modify nutrient and oxygen supply and clearance, and overall disrupt the homeostasis that would otherwise allow tumours to be targeted by the host immune system [4]. Of the milieu of cell subsets within a patient's TME, very little is understood of their interaction and how these associations may influence the outcome to immunotherapy.

While the field of immunology has benefited from flow cytometry to delineate the roles of cellular hierarchies found in peripheral blood, similarly high-plex methods to analyse both composition and spatial organization of cells in tissue have been lacking. As such, information garnered thus far has been limited to targeted multiplex immunohistochemistry (mIHC) panels to evaluate the prognostic and predictive value of small numbers of cell markers in parallel including $CD3^+$, $CD4^+$,

$CD8^+$, $FoxP3^+$, $PD-1^+$, $CD68^+$ and $PD-L1^+$ [11–14]. Interestingly, PD-L1 expression within the immune cell compartment is being increasingly reported and provides confounding evidence to the PD-1/PD-L1 paradigm of tumour-centric immune evasion [15–18].

Advances in multiplexed techniques to measure the composition of tumour and the TME have begun to unravel the cellular phenotypes that associate with therapy response. Here, we adopted a discovery approach to examine the cellular composition of lung cancer patient samples using spatial proteomic and transcriptomic methodologies to evaluate tumour and TME compartments independently, with additional single-cell level mIHC. A second line, retrospective ICI immunotherapy cohort (IO) was examined by targeted 1800 mRNA and 68 protein digital spatial profiler (DSP) assays, as well as 6-plex mIHC. We sought to use unbiased statistical approaches to inform upon on outcome to therapy, and to assess if these outcome associations were specific for treatment.

MATERIALS AND METHODS

This study has Queensland University of Technology Human Research Ethics Approval (#2000000494). Pre-treatment NSCLC tissue microarrays (TMAs) were constructed by TriStar Technology Group (USA) from retrospective cohorts in conjunction with their clinical collaborators. TMAs consisted of single 1 mm cores per tumour sample from patients who received second-line ICI immunotherapy (IO cohort) treatments. Pathologists reviewed whole sections prior to coring representative tumour regions for this assay. Serial sections of the IO cohort were analysed by Nanostring GeoMX DSP protein and mRNA panels (Cancer Transcriptome assay [CTA] Atlas panel), and by mIHC. Clinical endpoints included ICI response and OS according to RECIST 1.1 criteria. All patient clinicopathological, treatment, ICI response and survival parameters were recorded and provided by TriStar Technology Group and their medical teams.

Nanostring GeoMx Digital Spatial Profiler (DSP)

NSCLC TMA slides were stained and analysed by Nanostring GeoMx DSP system at the Systems Biology and Data Science Group at Griffith University (Gold Coast, Australia). Morphology/visualization markers consisted of CD3, CD68 and pan-cytokeratin. mRNA panel consisted of 1812 curated genes from the human CTA including housekeeping and negative control probes. Slides were processed and hybridized according to the manufacturer's instructions. Region of Interest (ROI) selection on each TMA core was performed such that 660 μm circles were segmented into cytokeratin⁺ (tumour) and cytokeratin⁻ (stroma) regions by thresholding on cytokeratin staining intensity. Barcodes from these regions were collected to generate measurements per compartment. Barcodes were sequenced, mapped and counted by next-generation sequencing (NGS) read-out as per manufacturer's instructions. Quality control (QC) was performed within the GeoMx DSP analysis suite to remove outlying probes and collapse counts from 5 probes per gene to single measurements. These QC data were output for downstream bioinformatic analysis.

The protein panel consisted of 68 antibodies including core panels across human immune cell profiling, IO drug target, immune activation, immune cell typing, pan-tumour, cell death and PI3K/AKT panels. Slides were processed as per manufacturer's instructions and tumour/stroma regions demarcated as above. Antibody barcodes were counted on Ncounter platform as per manufacturer's instructions and External RNA Controls Consortium (ERCC) QC performed in the GeoMx DSP analysis suite prior to outputting data for bioinformatic analysis.

Multispectral mIHC

Slides were stained using pre-validated MOTIF lung cancer PD-1/PD-L1 panel (Akoya Biosciences, USA) according to the automated mIHC staining instructions provided by the manufacturer for the Leica Bond RX (Leica Biosystems, USA) at the Walter and Eliza Hall Institute (WEHI) histology core (Melbourne, Australia) (<https://www.akoyabio.com/phenoimager/assays/motif-pd-1-pd-l1-panel-auto-luca-kit>). Antibodies were provided at ready-to-use (RTU) concentrations and staining was performed in the order below with corresponding Opal dye pairing: FoxP3 (D608R)—Opal 570, PD-L1 (E1L3N)—Opal 520, PanCk (AE1/AE3)—Opal 690, PD-1 (EPR4877)—Opal 620, CD8 (4B11)—Opal 480, CD68 (PG-M1)—TSA DIG, Opal 780. Staining was tested on tonsil

tissue for appropriate staining pattern prior to application on NSCLC tissue. Whole slide scans were performed on Vectra Polaris (Akoya Biosciences, US) by WEHI histology core, and images were spectrally unmixed in InForm (Akoya Biosciences, US) using MOTIF spectral libraries.

Image analysis

Image analysis and cell classification were performed in collaboration with Enable Medicine (USA). Nuclear cell segmentation was performed using DeepCell, followed by segmentation dilation [19, 20]. Cellular protein expression levels were computed from the mean Opal fluorophore intensity for each biomarker. Cell classification was performed by manually gating on fluorescence intensity to define positive cells in scatter plots of each channel relative to a control channel. Cells were then assigned to classes according to the rules-based phenotyping protocol supplied by the manufacturer: CD68⁺, (CD68⁺, PD1⁺), (CD68⁺, PD-L1⁺), CD8⁺, (CD8⁺, PD1⁺), (CD8⁺, FoxP3⁺), (CD8⁺, PD1⁺, FoxP3⁺), (FoxP3⁺, PD1⁺), PanCk⁺, (PanCk⁺, PD-L1⁺). A minimum threshold of 3000 cells was set for cores to include in mIHC spatial analysis. Cell frequency was defined by counting the instances of each cell class and normalizing to the total cell count for each core. Cell interactions were defined by shared edges of the Voronoi tessellation generated from the cell centres [21, 22]. Cell interaction frequencies were calculated by counting the instances of an interaction and normalizing to the total number of interactions in the core. Neighbourhoods were defined using the k-nearest neighbour algorithm (KNN). For each cell, the cell types of the 10 nearest neighbours were assigned as the features of that cell. These features were then run through an unsupervised KNN algorithm and assigned to 10 clusters. The choice of 10 nearest neighbours and 10 clusters was chosen heuristically as parameters that worked well for a wide variety of datasets [21, 22]. For cross-sample comparisons, the frequency of each cell type/interaction/neighbourhood was normalized against the highest frequency among the cores analysed. The cross-sample comparisons were used to generate dendrograms of cell frequencies/interactions/neighbourhood. *T*-tests were performed between response status groups for each of these metrics. These metrics were also assessed for OS associations by Cox proportional hazards models as continuous variables.

CD44 CO-detection by indexing staining

CO-detection by indexing (CODEX) (Akoya Biosciences, USA) staining including CD44 and PanCk was performed

by Enable Medicine, USA, as described. CD44 staining was performed using a commercially available oligo-conjugated antibody (CD44-BX005 (IM7) Akoya Biosciences) as per manufacturer's instructions. Briefly, formalin-fixed, paraffin-embedded (FFPE) tissue samples were mounted on 20 mm × 20 mm poly-lysine treated coverslips. The CD44 antibody was diluted 1:200 in a staining buffer. After antigen retrieval, 190 µL of antibody solution was added to the coverslips, which were incubated for 3 h at RT in a humidity chamber. This was followed by several cycles of washing and fixation steps. For a more detailed protocol, see Reference [23].

Coverslips were imaged on an inverted fluorescence microscope (Keyence BX-810) using a Plan Apo 20× 0.75 NA objective (Nikon). The CODEX imaging cycles were performed using a Codex Instrument (Akoya Biosciences). The RX-005 Atto-550 reporter (Akoya Biosciences) was used to tag the CD44 antibody. Large regions were broken up into tiled subregions, and 5 z-stack slices with a step size of 1.5 µm.

Images were deconvolved and pre-processed using image pre-processing pipeline (Enable Medicine, USA). Briefly, background signal was removed from the image by using a computationally aligned blank acquisition cycle as a reference channel. Then, image deconvolution was performed for each biomarker image z-stack, and the best focus was chosen using an extended depth of field algorithm. Finally, the individual tiles were aligned and stitched together, and all channels were stacked. CD44 mean fluorescence intensity was calculated within PanCK⁺ mask area and expressed as the geometric mean of pixel intensities normalized to the mask area in µm².

Data analysis

Transcriptomic and proteomic data qualities were evaluated by principal component analysis (PCA) and coefficients of variation (CV) assessed to determine the suitability of the RUV-III normalization method [24, 25]. Differential expression (DE) analysis was performed within DeSeq2 and Limma packages [26, 27]. Benjamini-Hochberg correction for multiple comparisons was used to adjust *p*-values for differential analysis and Cox proportional hazards analyses and are shown in supplementary data. Significant exploratory statistics shown in results are not adjusted for multiple comparisons as a result of our cohort sample size. The most predictive or discriminative signatures classifying ICI response were developed using sparse partial least squares-discriminant analysis (sPLS-DA) [28]. The performance of the sPLS-DA was assessed using 10-fold leave-one-out cross-

validation and misclassification error was investigated using balanced error rate (BER) and area under receiver operator characteristic (ROC) curves. Only highly stable features (>0.8) were included, and the final sPLS-DA model was limited to one variable per 2 samples. Cox proportional hazards survival analysis using continuous variables and not cut-point method was conducted within R studio [29] using the Survival package [30] and plots generated by ggplot2 [31]. Ingenuity Pathway Analysis (IPA[®]) was used to evaluate upstream regulators of differentially expressed transcripts (QIAGEN Inc., <https://www.qiagenbioinformatics.com/products/ingenuity-pathway-analysis>).

RESULTS

Patient cohorts

The patient cohort consisted of *n* = 41 advanced stage III-IV NSCLC patients who received ICI therapy in the second-line setting (Table 1), of which 39% were classified as responsive (R), while 61% were non-responsive (NR) according to RECIST 1.1 criteria. Anti-PD-1 therapies Nivolumab and Pembrolizumab comprised 94% of treatments, with one patient receiving anti-PD-L1 agent Durvalumab. Ninety-four percent and 32% of patients remained alive at follow-up time, for responsive, and NR groups, respectively. The cohort contained both squamous and adenocarcinoma NSCLC histology.

TABLE 1 Immunotherapy cohort (IO) cohort characteristics.

IO cohort	Non-responder, N = 25	Responder, N = 16
Gender		
Female	9 (36%)	5 (31%)
Male	16 (64%)	11 (69%)
Age ^a	66 (59, 69) ^a	58 (58, 63) ^a
ICI treatment		
Durvalumab	0 (0%)	1 (6.2%)
Nivolumab	22 (88%)	11 (69%)
Pembrolizumab	3 (12%)	4 (25%)
Current status		
Alive	8 (32%)	15 (94%)
Deceased	17 (68%)	1 (6.2%)
Histology		
Adenocarcinoma	12 (48%)	13 (81%)
Squamous cell carcinoma	13 (52%)	3 (19%)

^aBrackets for age show the range.

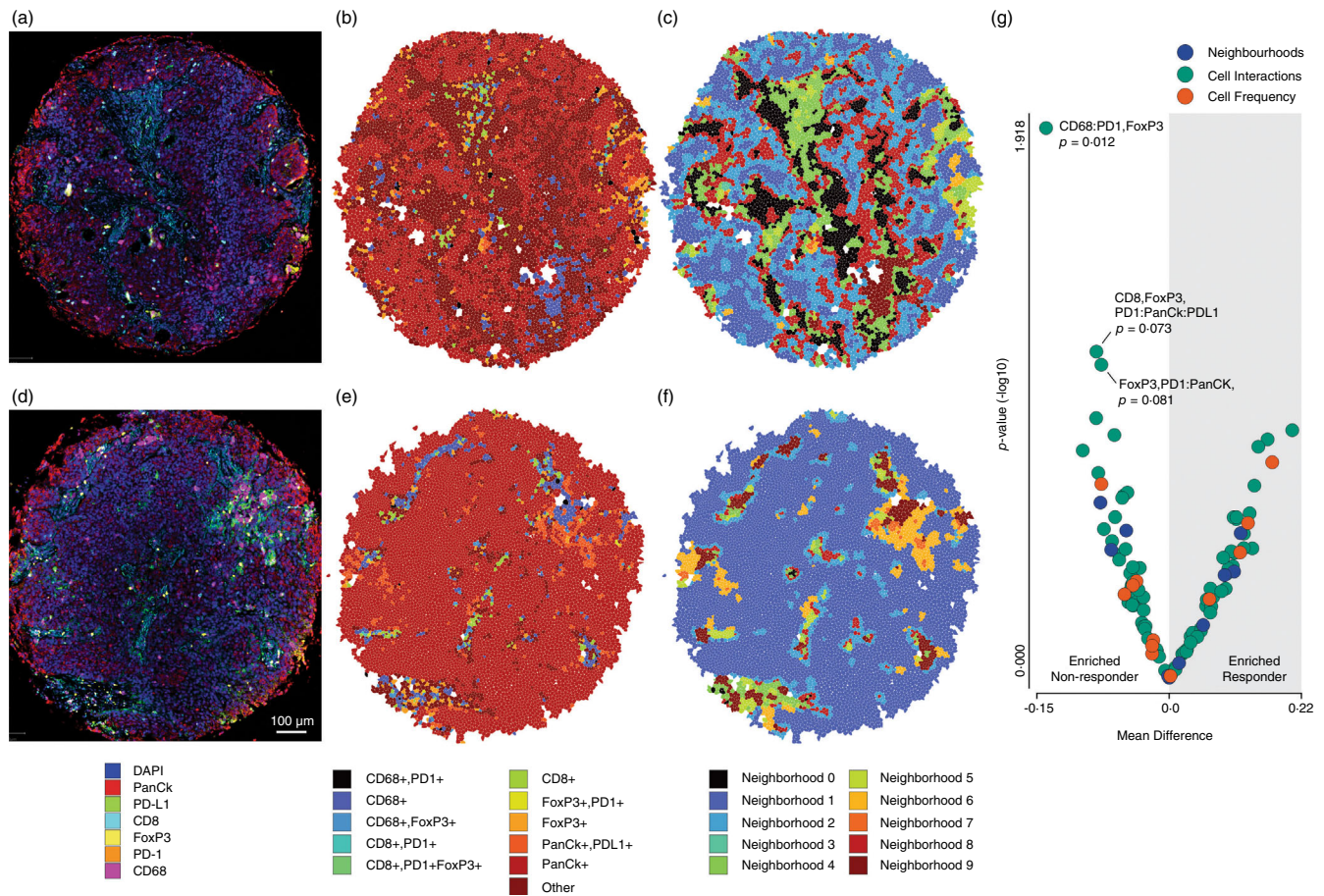


FIGURE 1 Multispectral spatial analysis revealed the enrichment of cellular interactions in immune checkpoint inhibitor (ICI) sensitive tumours. Representative analysis of tissue microarrays (TMA) cores from responders (a–c) and non-responders (d,f). A Representative non-small cell lung cancer (NSCLC) core from the responder. (b) Concordant cell-type Voronoi. (c) Concordant neighbourhood Voronoi. (d) Representative NSCLC core from non-responder. (e) Concordant cell-type Voronoi. (f) Concordant neighbourhood Voronoi. (g) Volcano plot indicating enrichment and significance of cell frequency, cell interaction and cellular neighbourhoods in responding/non-responding NSCLC cohorts.

Multiplex IHC spatial analysis

The current PD-L1 IHC companion diagnostic for PD-1/L1 axis ICI therapy remains limited, both in its clinical assessment and biological meaning [32]. Here, we utilized an optimized multispectral, mIHC assay [33] to evaluate the frequency and spatial associations of ICI targets PD-1/PD-L1, cytotoxic T cells (CD8), T-regs (FoxP3), and macrophages (CD68) (Figure 1a,d). Normalized cellular counts were assessed for each marker and their phenotypic subsets (e.g., CD8⁺, FoxP3⁺) according to the manufacturers rules-based phenotyping workflow (Figures 1b,e and S1a,b). Subsequently, pairwise cell:cell interactions were ranked by the frequency of their shared Voronoi edges (Figure S1c,d). Cellular populations were grouped into cellular neighbourhoods by their nearest neighbour associations as published [22] (Figures 1d,f

and S1e,f). Differential enrichment of each of these features was tested in ICI response groups (Figure 1g). Neither tumour nor immune cell expression of PD-L1, nor T-cell expression of PD-1 was enriched in the responding cohorts, and in fact, the frequency of any phenotype alone did not associate with response in our data. Significantly, however, the interactions between CD68⁺ macrophages and PD1⁺, FoxP3⁺ cells were enriched in ICI refractory tumours ($p = 0.012$), while a trend existed for the interaction between CD8⁺, PD1⁺, FoxP3⁺ exhausted T cells and PanCk⁺, PD-L1⁺ tumour cells in ICI resistant tumours ($p = 0.073$) (Figure 1g). KNN analysis (Figure 1c,f) did not indicate enrichment of cellular neighbourhoods described by the markers evaluated in this assay (Figures 1g and S1g). Of note, no features were observed to be enriched in ICI-responsive tumours in our cohort. Assessment of these features in IO cohorts by the

Cox proportional hazards model did not indicate significant associations with OS.

Digital spatial profiling

While targeted mIHC offers parallel spatial insights into tumour cellularity, it falls short of the depth required to tease apart the composition of complex tissues. Digital spatial profiling was therefore applied to better delineate the immune proteome and targeted transcriptome of the IO cohort tissues. Regions within tumour cores were segmented using cytokeratin/ non-cytokeratin immunofluorescent masks to enable transcriptome and proteomic marker measurement within the tumour and stroma compartments independently (Figure S2). In this way, the measurements obtained from tumour regions comprised both tumour cells as well as infiltrating host cell populations. Similarly, stromal regions described the cellular content of tumour-associated stroma. While most cores contained both tumour and stroma regions, some punches lacked sufficient stromal content for the mRNA assay. As such, of the 41 IO cohort samples, robust transcriptome data were obtained for 33 tumour ROIs and 23 stroma ROIs, which were matched for 21 patients, while protein measurements were complete in both cohorts due to the nature of antibody-based detection compared to that of NGS. The data were assessed for appropriate normalization to account for differences in assay input due to varying cellular densities. House-keeping normalization by assay house-keeping probes was compared to remove unwanted variation (RUV-III) [25] factor analysis which has been demonstrated to be more effective for variance stabilization than traditional normalization methods [34] (Figure S3). One outlying tumour region of the protein assay was excluded from the analysis.

Unsupervised dimension reduction was applied to explore the data's relationship with sample clinical features, including IO response, stage at diagnosis and NSCLC histology, however, variance across samples was not clearly attributable to these sample characteristics (Figure S4).

Postulated markers of IO response by DSP

To further test for associations of cellular markers postulated to be involved in IO response, we evaluated therapeutic targets PD-1 and PD-L1 [11, 16], tumour cell antigen presentation (HLA-DR) [35, 36] and cytotoxic T cells (CD8⁺) [12] in our data. Comparative analysis by DSP alongside our mIHC data indicated that these markers were not significantly associated with ICI

response in protein or mRNA DSP assays, despite a trend for a higher abundance of PD-1 and CD8 mRNA in tumour regions of ICI-sensitive patients (Figure S5).

Differential analysis of IO response

With this in mind, we sought to identify markers in our DSP data which better discriminated ICI response. Differential analysis was performed between responders (R) and non-responders for protein markers in tumour regions (R [*n*] = 15, NR [*n*] = 24), stromal regions (R [*n*] = 16, NR [*n*] = 24), as well as mRNA in tumour (R [*n*] = 15, NR [*n*] = 19), and stroma (R [*n*] = 8, NR [*n*] = 18) regions (Figure 2, Table S1).

This analysis indicated that IL-2 receptor alpha (CD25) was upregulated ($p = 0.028$) in tumour regions of responding patients (Figure 2a), which also corresponded with higher levels of *IL-2* mRNA ($p = 0.001$) within these patients' stroma (Figure 2d), suggesting key conditions for ICI efficacy. Natural killer cells (CD56) ($p = 0.005$) and immuno-inhibitory markers CTLA4 ($p = 0.021$), IDO1 ($p = 0.023$) were lower in responders' stroma (Figure 2c), while levels of GITR ($p = 0.01$), CD4 ($p = 0.01$), CD56 ($p = 0.04$), PD-L2 ($p = 0.04$), CD44 ($p = 0.02$) and *CD24* mRNA ($p = 0.0008$) were also lower in their tumour regions (Figure 2a, b). Interestingly, the expression of CD44 receptor in tumour regions shared an inverse relationship with the mRNA of one of its stromal ligands, *SPP1* (osteopontin). Significantly more *SPP1* mRNA ($p = 0.008$) was observed in the stroma of responding patients (Figure 2d), while its tumour cell receptor, CD44, was relatively depleted in these patients. Decreased PTEN was associated with response in both tumour ($p = 0.02$) and stroma ($p = 0.02$). Surprisingly, EPCAM protein ($p = 0.01$) was highly abundant within the stroma of responding patients, and its stromal expression appeared specific as evidenced by a lack of concordant epithelial cell marker, pan-cytokeratin.

IL2 is a key cytokine with pleiotropic results on immune cell recruitment, activation and survival. To investigate the cell phenotypes potentially being influenced by IL2 production, correlations between stromal *IL2* mRNA and concordant stromal protein marker data were evaluated (Figure S6). Interestingly, pro-apoptotic markers cleaved caspase 9 ($R = 0.73$, $p = 2e^{-5}$) and BAD ($R = 0.63$, $p = 5.5e^{-4}$) as well as the IL7 receptor (CD127) ($R = 0.52$, $p = 7e^{-3}$) and IL2 receptor (CD25) ($R = 0.53$, $p = 5e^{-3}$) were positively associated with levels of IL2 mRNA and thus ICI response, while levels of memory T cells (CD45RO) ($R = -0.62$, $p = 7e^{-4}$) possessed an inverse association.

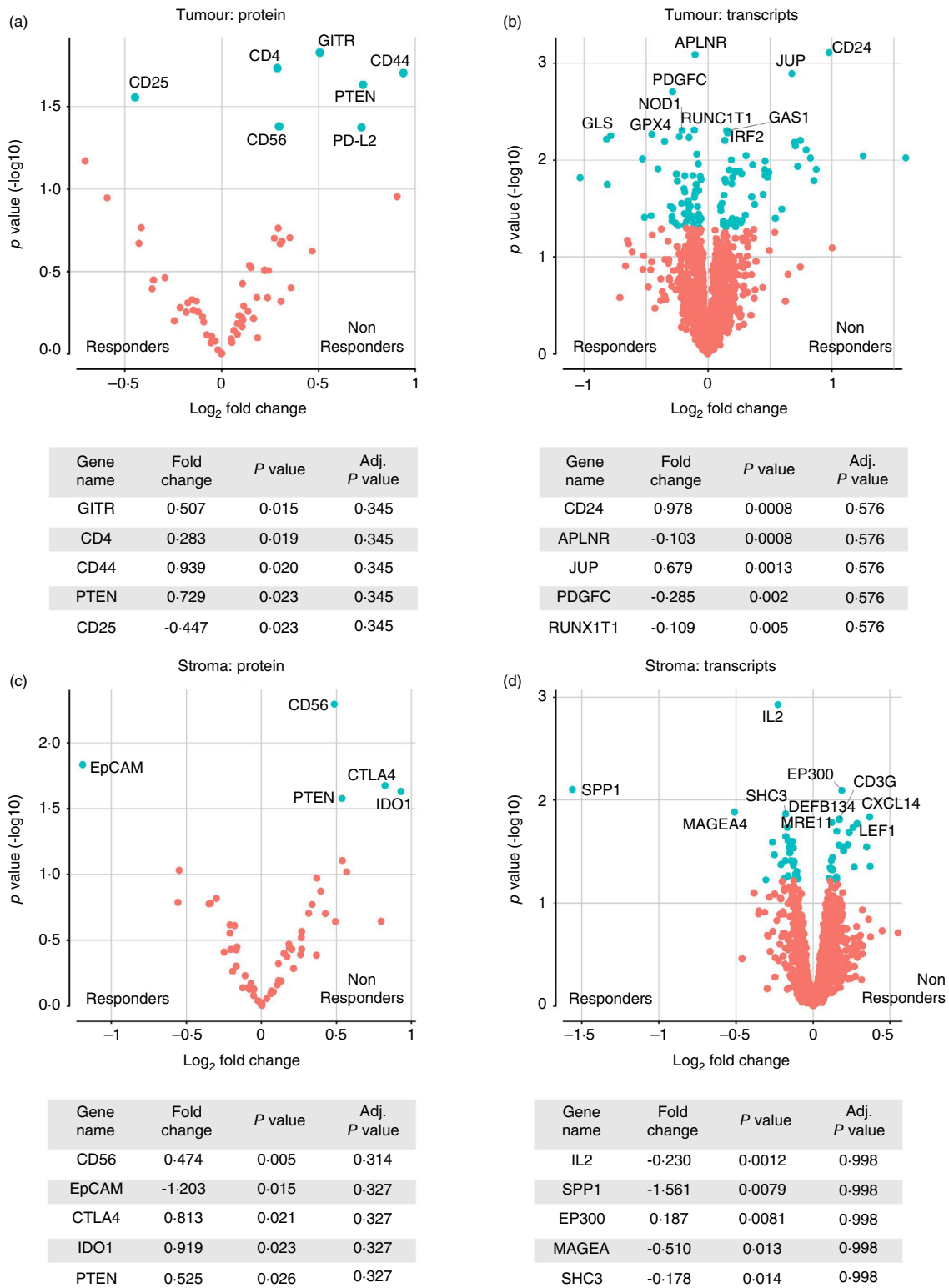


FIGURE 2 Differential expression of protein and mRNA features by immune checkpoint inhibitors (ICI) response. (a) Volcano plot of DE proteins in tumour. (b) Volcano plot of differential expression (DE) mRNAs in tumour. (c) Volcano plot of DE proteins in stroma. (d) Volcano plot of DE mRNAs in stroma. Tables indicating most significant DEs shown. Negative value indicates upregulation in responding patients. Differential expression was performed by immunotherapy cohort (IO) response status within DESeq2 using remove unwanted variation (RUV) normalized data. Adjusted *p*-value show Benjamini–Hochberg multiple testing correction.

Differential CD44 expression is tumour cell specific

While tumour/stroma compartmentalization has helped to overcome previous generations of bulk analysis technologies, it lacks the ability to assign markers to their parental cell type. We employed multiplex immunofluorescence by CODEX to validate tumour cell CD44 expression in a serial section of the IO cohort. CD44 expression was found on tumour cells as well as infiltrating stromal cells (Figure 3a,b). PanCK masks were used to compartmentalize the mIF image and the geometric mean of fluorescence intensity for CD44 was calculated per tumour mask area to normalize for cell abundance and to parallel DSP assay output. Expression of CD44 on positive tumour cores appeared homogenous across tumour cells. Comparison between CODEX data (Figure 3c) shows concordance with CD44 DSP protein data (Figure 3d) and with a negative association with ICI response. In addition, a linear correlation between CD44 DSP counts and CD44 mean fluorescence (R = 0.61) (Figure 3e) exists in support of DSP target discovery.

Survival analysis

Differentially expressed features within the IO cohort were further examined for their associations with survival outcomes (Figure 4, Table S2). Enrichment of tumour CD44 (hazard ratio [HR] = 1.6, $p = 0.01$) and stromal CTLA4 (HR = 1.78, $p = 0.003$) and CD56 (HR = 1.58, $p = 0.07$) markers in ICI refractory patients corresponded with poorer OS (Figure 4a). Interestingly, non-DE proteins including IL2 mRNA correlate, proapoptotic BAD (HR = 0.5, $p = 0.01$), and MDSC/M2 macrophage ARG1 (HR = 2.37, $p = 0.01$) markers were associated with improved and poorer outcome, respectively (Table S2). Twenty-nine of 109 DE tumour transcripts, as well as 4 of 41 DE stromal transcripts, exhibited survival associations (Table S2). Segregation of these DE transcripts by their up or down regulation in ICI-responsive patients indicated an inverse association (Figure 4b, c). Downregulation of several transcripts corresponded with significantly poorer outcomes, including stromal E-selectin (SELE) (HR = 652, $p = 8.8e^{-4}$) and T-cell recruitment chemokine CCL17 (HR = 70, $p = 0.006$)

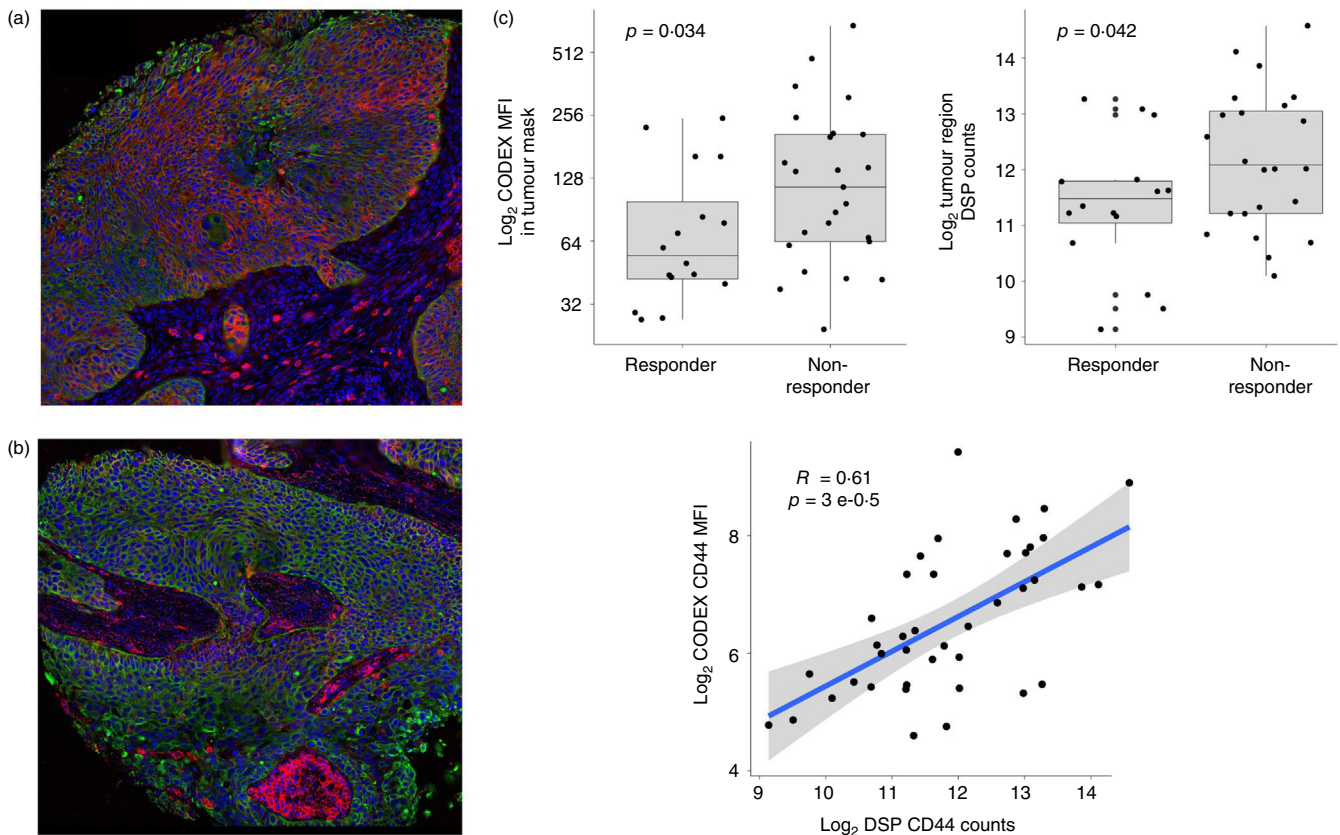
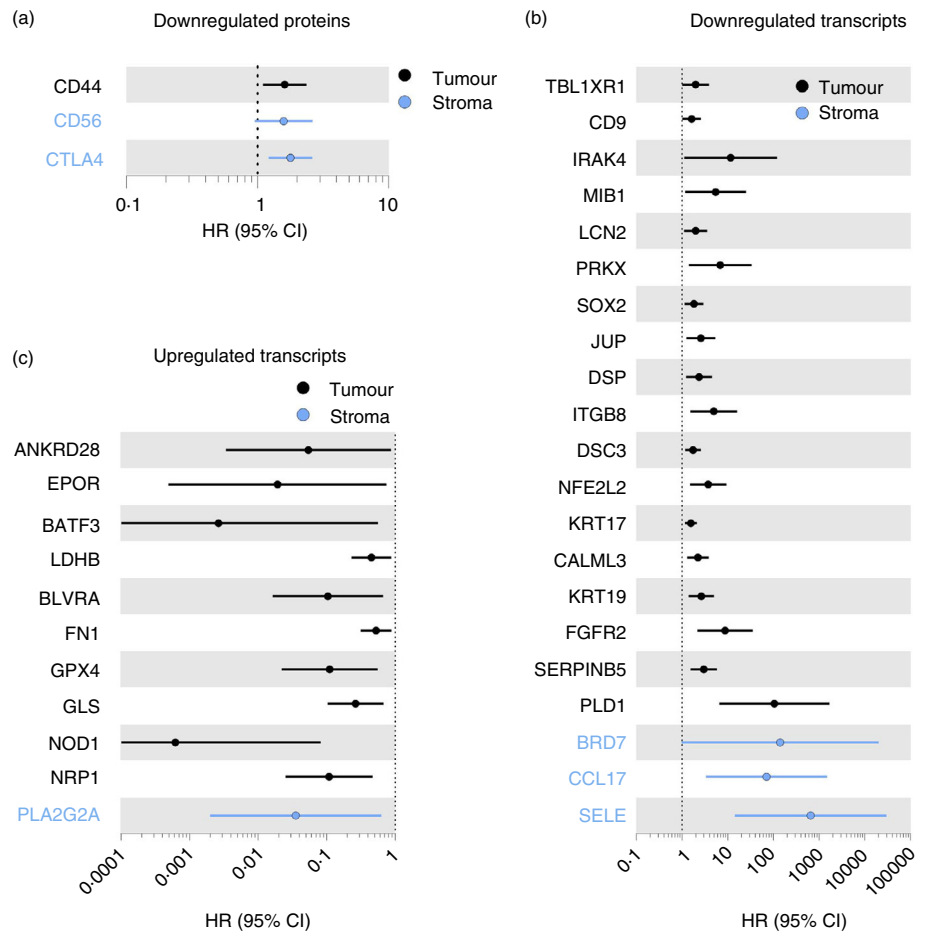


FIGURE 3 Validation of tumour CD44 expression by CO-detection by indexing (CODEX) multiplex immunofluorescence. (a) Representative CD44 staining (Red) in tumour cells (Green) in non-responder tumour. (b) Representative CD44 staining (Red) in tumour cells (Green) in responder tumour. (c) Geometric mean fluorescence intensity (mFI) of CD44 by CODEX in responders and non-responders. (d) Log2 CD44 digital spatial profiler (DSP) counts in responders and non-responders. (e) Correlation between CODEX mFI and DSP counts.

FIGURE 4 Cox proportional hazard survival analysis of differentially expressed protein and mRNA features by immune checkpoint inhibitors (ICI) response. (a) Forest plot showing hazard ratio (HR) and 95% confidence interval (CI) of downregulated proteins. (b) Forest plot showing HR and 95% CI of downregulated transcripts. (c) Forest plot showing HR and 95% CI of upregulated transcripts.



(Figure 4b). Interestingly, while stromal MTOR expression was not associated with response, it was highly associated with poor outcome (HR = 1065, $p = 0.008$) (Table S2). Conversely, enrichment of DE transcripts in ICI-responsive patients corresponded with significantly enhanced OS, including stromal PLA2G2A (HR = 0.03, $p = 0.02$), and tumour NRP1 (HR = 0.1, $p = 0.002$), and NOD1 (HR = $6e^{-4}$, $p = 0.003$) (Figure 4b). Taken together, these results indicate the association of these biomarkers with both ICI response and OS outcome following treatment.

Multivariate modelling of IO response

While the differential analysis was key in resolving distinguishing features of our data relative to ICI response, their multivariate integration may yield an improved diagnostic signature. Multivariate modelling was performed by sparse partial least squares-discriminant analysis (sPLS-DA). PLS-DA offers a feature selection method to identify the most discriminative factors in a dataset that are able to classify samples in a supervised framework, that is, samples labelled by ICI response [28].

sPLS-DA performs internal validation by leave-one-out 10-fold cross-validation with lasso penalisation for optimal feature selection, and the number of features was limited to one per 2 samples. Features within protein (Figure 5) and mRNA (Figure 6) data were able to efficiently stratify ICI response within tumour and stroma compartments as demonstrated by patient sample separation on components 1 and 2 of the sPLS-DA model (Figures 5 and 6a,b).

Within tumour regions, responding patients could be characterized by lower levels of CD4, and PTEN (AUC = 0.84) (Figure 5c) with a secondary signature comprised of lower levels of fibronectin, CD56, Ki-67, CD44 and ER α (AUC = 0.95) (Figure 5d). Furthermore, mRNA of responding tumours were characterized by higher *APLN*R (AUC = 0.87) (Figure 6c). A secondary tumour mRNA signature comprised reduced *NKX2-1*, *SOX2*, *KRT6*, *GLS*, *PTCH1* and *CALM3* (AUC = 1) (Figure 6d).

Stromal protein markers that indicated IO response comprised higher levels of EpCAM and reduced CD56, CTLA4, IDO1, PTEN, ARG1, GZMA (AUC = 0.9) (Figure 5e), with a secondary signature composed of increased ER-alpha, GITR and CD20 (AUC = 0.94) (Figure 5f).

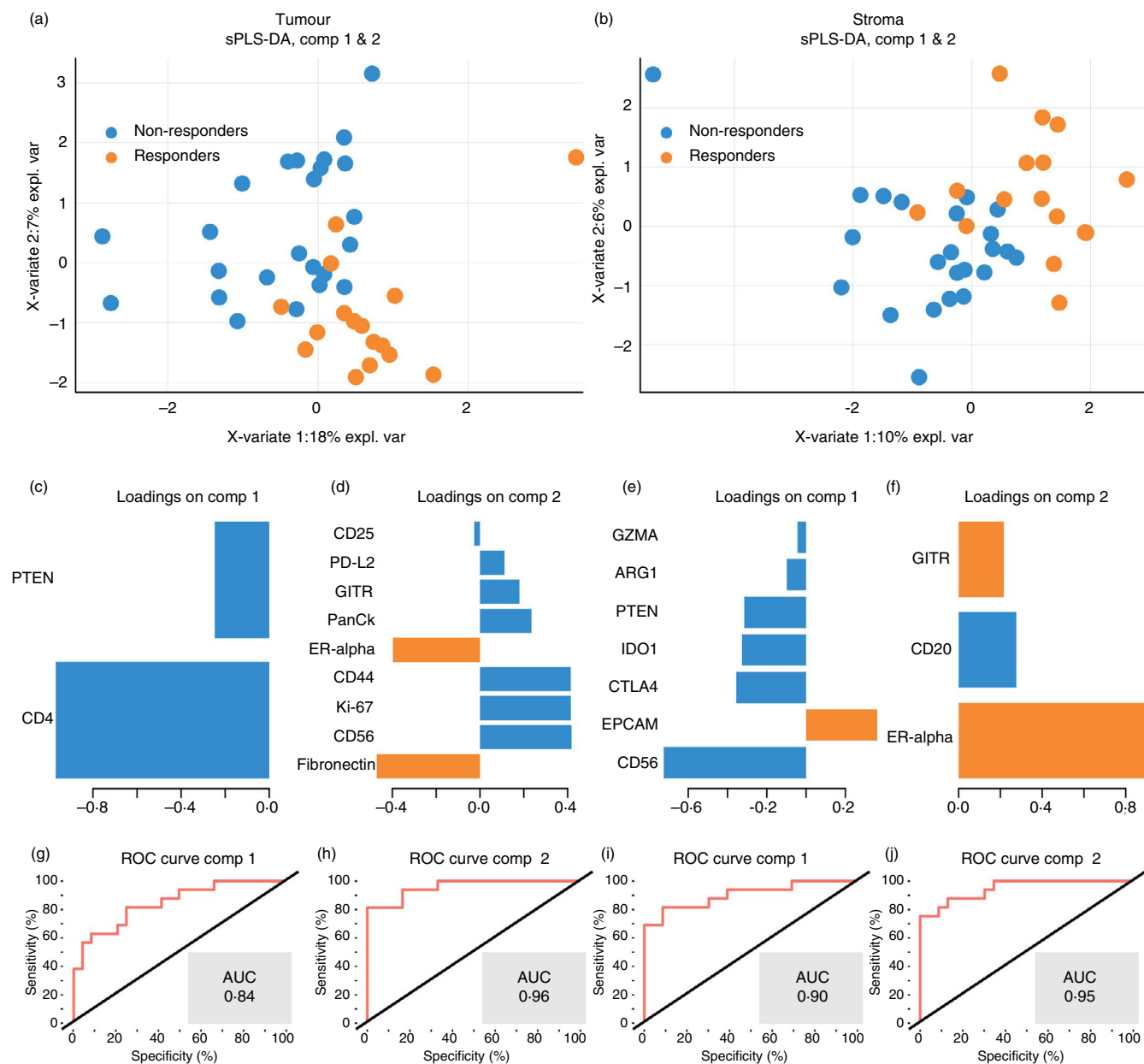


FIGURE 5 Multivariate sparse partial least squares-discriminant analysis (sPLS-DA) of protein features that distinguish non-small cell lung cancer (NSCLC) immunotherapy cohort (IO) response. Patient sample discrimination defined by Components 1 and 2 of sPLS-DA model for tumour (a) and stroma (b). (c) Component 1 loading for tumour regions. (d) Component 2 loading for tumour regions. (e) Component 1 loading for stroma. (f) Component 2 loading for stroma. (g) Receiver operator characteristic (ROC) curve to evaluate Component 1 tumour signature. (h) ROC curve to evaluate component 2 tumour signature. (i) ROC curve to evaluate Component 1 stroma signature. (j) ROC curve to evaluate Component 2 stroma signature. Colour of component loadings indicates patient group in which feature was maximally expressed. Positive or negative values in bar chart indicate positive or negative loading to the discriminant signature. Blue = non-responder, Orange = responder.

Interestingly, *IL2* RNA alone solely formed component 1 of the stromal signature (AUC = 0.9) (Figure 6e), while reduced *COL4A6* composed the component 2 signature (AUC = 0.98) (Figure 6f).

Indications from the sPLS-DA together with results of the differential analysis provide evidence for the role of stromal *IL2* in the efficacy of PD1/L1 ICI therapy.

In addition, lower levels of natural killer cells (CD56) and IDO1 in both tumour and stroma were associated with response. Interestingly, the sPLS-DA model identified that stromal *COL4A6* (collagen type IV) expression within the ICI-resistant group contributed significantly to the discriminant signature, indicating their potential importance in refractory disease.

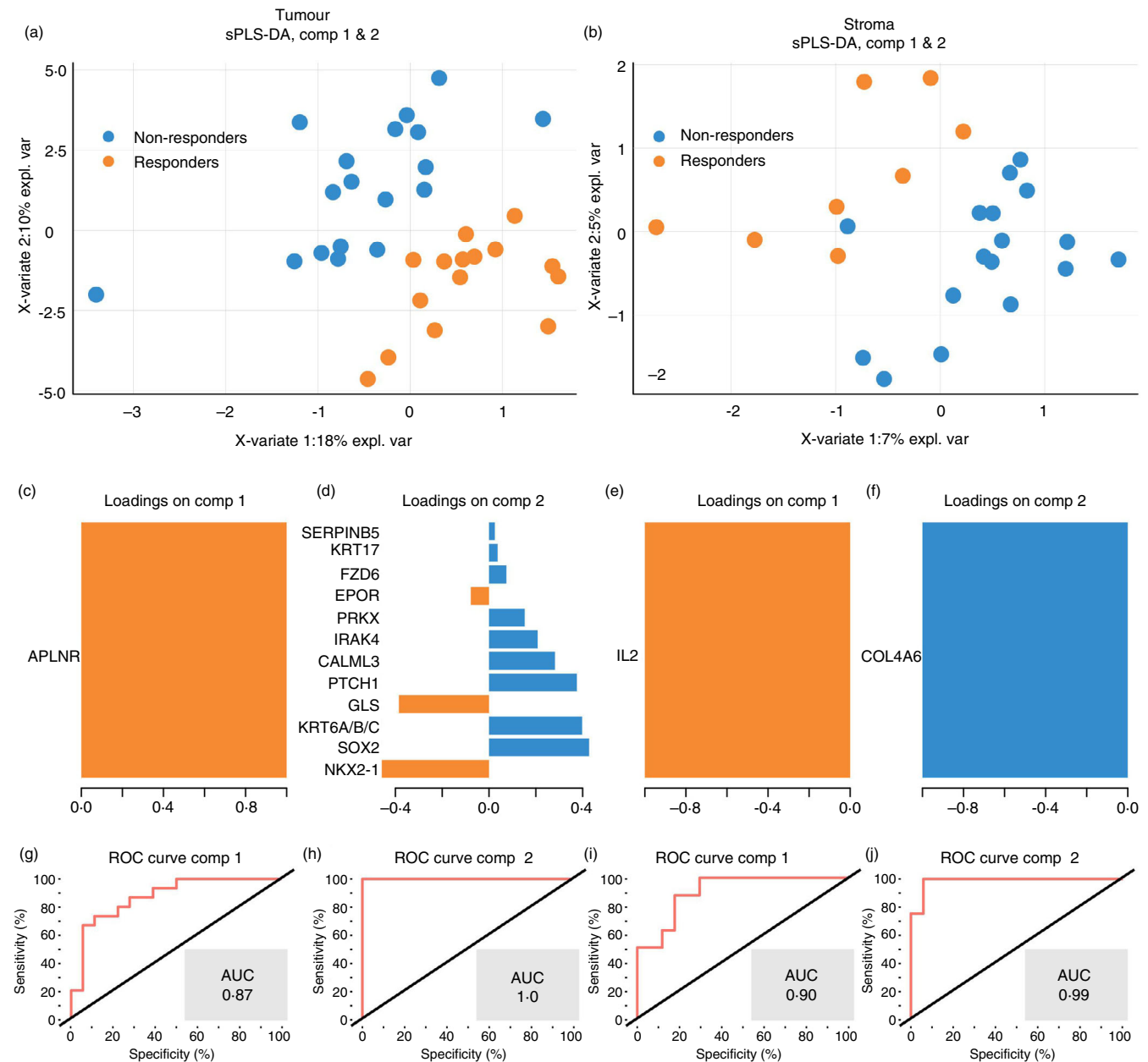


FIGURE 6 Multivariate sparse partial least squares-discriminant analysis (sPLS-DA) of mRNA features that distinguish non-small cell lung cancer (NSCLC) immunotherapy cohort (IO) response. Patient sample discrimination defined by Components 1 and 2 of sPLS-DA model for tumour (a) and stroma (b). (c) Component 1 loading for tumour regions. (d) Component 2 loading for tumour regions. (e) Component 1 loading for stroma. (f) Component 2 loading for stroma. (g) Receiver operator characteristic (ROC) curve to evaluate Component 1 tumour signature. (h) ROC curve to evaluate Component 2 tumour signature. (i) ROC curve to evaluate Component 1 stroma signature. (j) ROC curve to evaluate component 2 stroma signature. Colour of component loadings indicates patient group in which feature was maximally expressed. Positive or negative values in bar chart indicate positive or negative contribution to the discriminant signature. Blue = non-responder, orange = responder.

Network and cellular inference

Ingenuity Pathway Analysis© (IPA®) was used to infer the molecular pathways associated with differentially expressed genes (DEGs) in responding patients. Stromal DEG's indicated the potential suppression of IFN γ activity (activation score -2.22 , $p = 0.0254$) in responders, evidenced by the

downregulation of several of its downstream transcriptional products in our data including *CASP3*, *CCL17*, *DDX58*, *HLA-DQB1*, *IFTM1*, *PROM1*, *SELE* and *VCAM1* (Figure S8a). Tumour DEGs also implicated the inhibition of oestrogen receptor (ER) (activation score -2.891 , $p = 0.013$) and Wnt-1 (CCN5) (activation score -2.45 , $p = 0.003$) signalling pathways in responding patients (Figure S8b,c).

DEG enrichment within the nanostring CTA pathway annotations showed some associations with the dysregulation of PI3K/Akt signalling, differentiation, MAPK signalling, cell adhesion and motility, oxidative stress, interleukin signalling, and GPCR signalling in tumour regions (Table S3). Similarly, stromal DEGs were represented in chemokine, GPCR and MAPK signalling pathways (Table S3).

SPP1 mRNA (osteopontin) was the most highly enriched transcript ($\text{Log}_2 \text{FC} = 1.5$) in ICI-responsive patients. We therefore sought to assign the cellular source of this transcript in published NSCLC single-cell RNAseq data that described 9 distinct cell lineages in NSCLC tissue, including the immune cell subsets (T, NK, B, myeloid, MAST) in addition to epithelial cells, fibroblasts and endothelial cells (GSE131907) [37]. We observed overrepresentation of *SPP1* within the myeloid cell lineage (cluster 1), with more specific expression within monocyte-derived macrophages (cluster 5) (Figure S7). The enrichment of *SPP1* mRNA comes despite the absence of increased parental myeloid and macrophage cell markers in our data, including CD11c, CD163 and CD68 (Table S1), suggesting myeloid activation and secretion of soluble osteopontin is more directive in ICI response than cellular infiltration alone.

DISCUSSION

The composition of NSCLC tumours and the interactions that occur at their stromal interface to influence disease progression and ICI response is unclear. Current therapeutic paradigms to reinvigorate cytotoxic anti-tumour responses are hampered by both T-cell exhaustion and additional immunosuppressive signals within the TME that predispose a patient's resistance to therapy. Our study is among the first to characterize these phenomena in both tumour and stromal tissue compartments and provide simultaneous high-plex insight into the in-situ biology of NSCLC patients that subsequently received ICI.

The novelty of this approach for biomarker discovery, however, comes with several limitations inherent in emerging clinical questions when combined with cutting-edge technologies.

The limited size, retrospective nature of our cohort, as well as the use of single TMA core samples per patient means that the findings presented here require extensive validation. In addition, region of interest-based assays only provide a snapshot of tumour content. Thus, validation must be performed in prospective cohorts with orthogonal imaging technologies to delineate the cell subtypes responsible for ICI response phenotypes.

Limitations notwithstanding, we employed state-of-the-art techniques to profile NSCLC tumours to gain an understanding of the underlying tissue architecture. Overall, the combination of our findings from mIHC, protein and mRNA differential analysis illustrates the landscape of the TME to be consistent with our current understanding of the immune response with several novel findings. We discuss some of these findings in the context of their current implications within the field, and emphasize the discovery nature of this study that serves to open several routes to understand the influence of the TME upon ICI outcome.

Our observation that the interaction between CD68⁺ macrophages and PD1⁺, FoxP3⁺ cells is enriched in ICI refractory tumours, independently of their frequency, is of interest. Tumour-associated macrophages (TAMs) have been implicated in both anti-tumour (M1 subtype, promote CD4/CD8 expansion) and pro-tumour functions (M2 subtype, CD163⁺, secrete ARG1 to dampen CD8 response) [38]. The function of PD1 expression on FoxP3⁺ Treg cells is poorly defined, however is suggested to mark a dysfunctional Treg state that expands upon PD1 blockade to overwhelm anti-PD-1 effect on PD1⁺ effector T cells, thereby contributing to resistance to ICI therapy [39, 40]. The functional implication for the interaction between this Treg subset and CD68 macrophages in our data requires further investigation, however, recent studies have indicated that M2 TAMs may interact with T cells to prevent their migration and infiltration into tumour islets [41], and we may be observing a different iteration of this interaction in ICI resistant tumours. Thus, the interactions between immune populations are indicative of the signalling that occurs to drive macroscopic phenotypes and supports the importance of the next generation of biomarkers that overcome reliance on cell abundance alone.

Within the GeoMx DSP data, analysis of the stroma indicated that CD56, CTLA4 and IDO1 were significantly associated with resistance to ICI therapy. IDO1 has been shown to be a driver of tumour progression in NSCLC [42]. It acts to deplete tryptophan, which is required for CD8 T-cell proliferation and activation, and acts to reduce CD4 T helper survival [43], and is thus an attractive target to sensitize patients to ICI. CTLA-4 is a master inhibitor of T-cell activation responsible for regulating self-tolerance, a process which is co-opted in immune evasion [44] and was thus the target of first-generation ICIs which displayed higher adverse events relative to current PD-1 blockade [45]. Interestingly, EPCAM was also enriched in stroma of responding patients, and is a novel finding that requires further validation, and provides a confounding observation to that made for tumour adjacent stromal EPCAM expression and its association

with more aggressive prostate cancer [46]. Lower tumour abundance of protein markers GITR, CD4, CD44, CD56 and PD-L2 but not PD-L1 was significantly associated with response. The findings that NK cell marker, CD56 as well as CD4 marker were associated with ICI resistance require further validation. CD56 within the panel is a poor marker of NK cells, and similarly, CD4 cell subtyping is required to draw conclusions about their roles in ICI response.

In addition, we demonstrate by mIF that tumour cell CD44 expression is upregulated in ICI refractory tumours, and is consistent with DSP data. CD44 is a hallmark of cancer cell “stemness” that promotes cancer cell survival and proliferation [47], and its expression has also been demonstrated to regulate tumour cell PD-L1 expression in vitro [48]. The association between tumour cell CD44 expression and refractory disease, particularly with its implication for therapeutic targeting to overcome ICI resistance is a novel finding of this study, and is consistent with recent literature for its specific role in immunotherapy response [49].

ICI responders demonstrated increased IL2 receptor alpha (CD25) with concordant mRNA expression of its cytokine ligand within the stroma. While our data do not discern the cellular source of CD25 in tumour regions (i.e., by concomitant increase in Treg markers CD4, FoxP3), it is curious to note the existence of this IL2 axis between tumour and stroma compartments. Taken together with the positive correlation between IL2 mRNA and pro-apoptotic markers cleaved caspase 9 and BAD, it is likely that endogenous levels of this cytokine have key roles in recruiting and sustaining the prerequisite cell phenotypes for ICI efficacy by balancing T-cell status and activity.

Interleukin-2 is a potent cytokine that has pleiotropic effects on the immune system including Treg maintenance, T-cell differentiation, CD8 T-cell expansion and cytotoxic activity of CD8 and NK cells. Its small but significant upregulation within tumour-associated stroma in our data may indicate fertile ground for immune cell survival and tumour clearance. Indeed, the correlation between stromal *IL2* expression and apoptotic markers is indicative of its pro-cytotoxic role in anti-tumour immunity. IL2 is produced largely by antigen-stimulated CD4⁺ cells, while also produced by CD8, NK and activated DCs. Synergistic activity of IL2 with PD-1 checkpoint inhibition has been demonstrated to enhance CD8 expansion and clearance of pre-clinical viral infection models [50] by inducing CD127⁺ and CD44⁺ memory T-cell phenotype despite concomitant increase in T-regs. Low-dose IL2 has been successfully used to enhance T-cell responses in the treatment of renal cell carcinoma and metastatic melanoma [51, 52] however is subject to variable patient tolerance. More recent work to develop a masked IL2 cytokine that is proteolytically cleaved and

activated by tumour-associated MMPs to promote CD8 cell expansion and overcome resistance to ICI has been demonstrated [53]. Similarly, a tumour targeting recombinant antibody linked to IL2 that localizes to tumour cells has been shown to induce cytotoxic CD8 expansion and overcome resistance to ICI [54]. Thus, we provide here exciting supporting evidence for the therapeutic value of IL2 within the TME and its requirement in the efficacy of PD-1/L1 ICI therapy.

Of note, limited other mRNAs were upregulated in responders but included *SPP1* which was highly enriched in the stroma of responding patients, along with small increases in *SHC3* and *MAGEA4*. The relative enrichment of the cytokine *SPP1* (osteopontin) mRNA within stroma of responding patients (Log₂ FC 1.5) in our data is novel and suggests that it may have an important role in generating an ICI-sensitive niche in tumours. It is curious to note that an inverse association appears between high stromal *SPP1* expression and low expression of tumour cell receptor pair, CD44, in ICI-sensitive patients, for which the potential mechanistic link requires further investigation.

Through publicly available scRNAseq data, we show that *SPP1* is highly enriched within monocyte-derived macrophage populations and may indicate the specific secretion of this cytokine by activated macrophages. In addition, *SPP1* is thought to be secreted by CD11b⁺ myeloid cells and has been implicated as an immune suppressor that inactivates the cytotoxic activity of CD8 T cells through interaction with the immune CD44 receptor [55]. Within LUAD TCGA data, *SPP1* expression was higher in EGFR mutant NSCLC tumours, and was associated with poorer prognosis, with GSEA indicating immunosuppression in high *SPP1* expression group with lower CD8 infiltration and higher M2 macrophage infiltration [56]. Similarly, evidence exists for an *SPP1*⁺ macrophage—fibroblast structure in hepatocellular carcinoma that inhibits the efficacy of PD1 blockade [57].

Conversely, it has also been shown to interact with both beta integrins and CD44 on proinflammatory T helper cells. This drives IL-17 production while suppressing IL-10, in addition to inducing the hypomethylation of IFN γ , promoting its production by T cells, thereby enhancing immune cell survival [58]. Its upregulation in our data suggests its role is more closely aligned with the latter function and highlights the dichotomous roles that cytokines may have in regulating immune cell activation and survival depending on cellular context.

The implication by gene set enrichment that IFN γ activity is suppressed in the pre-treatment TME of ICI-responsive patients provides a novel, if confounding, insight for the role of this pleiotropic cytokine. IFN γ is typically produced by immune cell subsets including T-cell, NK, T-regs and B cells, however, its distinct

activities are modulated by the profile of co-secreted soluble cytokines, including IL2. IFN γ has been shown to suppress T-reg activity to allow the expansion of T cells and promote PD-1 response in mouse models [59]. Indeed, a distinct dysregulated CD8⁺ TIL population in the TME that demonstrated higher levels of activation, proliferation and apoptosis with decreased IFN γ production was recently discovered [60]. The presence of such IFN γ suppressed cells associated with advanced clinical stage and ICI resistance in both clinical and pre-clinical samples.

Contrarily, IFN γ has also been shown to prevent CD8 expansion [61] and promote T-cell apoptosis [62], and thus has dichotomous roles. Exhausted CD8 T cells also lose secretion of IL2 and IFN γ and feature low proliferation and high expression of inhibitory markers including PD1, LAG3, TIM-3 [63]. Thus, ICI therapies targeting PD-1 typically induce IFN γ through reinvigoration of T cells and activation NK cells. Our data may provide a snapshot of the pre-treatment TME, whereby IFN γ suppression prevails, and marks the cellular environment that is thereby predisposed to more effectively activate upon ICI treatment.

Overall, our study forms a unique insight into the properties of NSCLC tumours prior to ICI therapy, and discerns features that distinguish subsequent patient response. The ability to measure both the immune proteome and transcriptome of FFPE tumour tissue routinely taken during biopsy or resection provides an opportunity to study tumour cellularity at unprecedented depth. We show here in a pilot cohort the strength of such applications in delineating the cues responsible for patient outcome. We identify that while cellular infiltration alone in TMA cores does not associate with ICI response, several key conditions may be required for a robust immune activation upon ICI treatment. While further interrogation and validation of several findings here are required to make conclusive observations, our study forms a basis for the application of next-generation technologies for the next generation of diagnostic pathologies.

ACKNOWLEDGEMENTS

The authors acknowledge the researchers in the Systems Biology and Data Science Research Facility (Griffith University), the Walter and Eliza Hall Institute (WEHI) histology core and Enable Medicine. This research was carried out at the Translational Research Institute, Woolloongabba, QLD 4102, Australia. The Translational Research Institute is supported by a grant from the Australian Government. Open access publishing facilitated by The University of Queensland, as part of the Wiley - The University of Queensland agreement via the Council of Australian University Librarians.

FUNDING INFORMATION

This work is supported by project grants and fellowships for Arutha Kulasinghe from NHMRC (1157741), Cure Cancer (1182179), the PA Research Foundation (Ken O'Byrne), and an International Association for the Study of Lung Cancer Foundation (IASLC) Foundation Award (Mark N. Adams).

CONFLICT OF INTEREST STATEMENT

Milan Bhagat and Marie Cumberbatch are employed by Tristar technologies. Aaron Mayer and Nicholas Matigian are employed by QCIF Bioinformatics. Aaron Mayer and Honesty Kim are employed by Enable Medicine.

DATA AVAILABILITY STATEMENT

The data that support the findings of this study are openly available in Geo at <https://www.ncbi.nlm.nih.gov/geo>, reference number GSE221733, GSE221322.

ORCID

James Monkman  <https://orcid.org/0000-0002-7219-8402>

Arutha Kulasinghe  <https://orcid.org/0000-0003-3224-7350>

REFERENCES

1. Sung H, Ferlay J, Siegel RL, Laversanne M, Soerjomataram I, Jemal A, et al. Global cancer statistics 2020: GLOBOCAN estimates of incidence and mortality worldwide for 36 cancers in 185 countries. *CA Cancer J Clin.* 2021;71(3):209–49.
2. Brueckl WM, Ficker JH, Zeitler G. Clinically relevant prognostic and predictive markers for immune-checkpoint-inhibitor (ICI) therapy in non-small cell lung cancer (NSCLC). *BMC Cancer.* 2020;20(1):1185.
3. Sadeghi Rad H, Bazaz SR, Monkman J, Ebrahimi Warkiani M, Rezaei N, O'Byrne K, et al. The evolving landscape of predictive biomarkers in immuno-oncology with a focus on spatial technologies. *Clin Transl Immunology.* 2020;9(11):e1215.
4. Sadeghi Rad H, Monkman J, Warkiani ME, Ladwa R, O'Byrne K, Rezaei N, et al. Understanding the tumor microenvironment for effective immunotherapy. *Med Res Rev.* 2021; 41(3):1474–98.
5. Davis AA, Patel VG. The role of PD-L1 expression as a predictive biomarker: an analysis of all US Food and Drug Administration (FDA) approvals of immune checkpoint inhibitors. *J Immunother Cancer.* 2019;7(1):278.
6. Cheng DT, Mitchell TN, Zehir A, Shah RH, Benayed R, Syed A, et al. Memorial Sloan Kettering-integrated mutation profiling of actionable cancer targets (MSK-IMPACT): a hybridization capture-based next-generation sequencing clinical assay for solid tumor molecular oncology. *J Mol Diagn.* 2015;17(3):251–64.
7. Samstein RM, Lee CH, Shoushtari AN, Hellmann MD, Shen R, Janjigian YY, et al. Tumor mutational load predicts survival after immunotherapy across multiple cancer types. *Nat Genet.* 2019;51(2):202–6.

8. Li Y, Chen Z, Wu L, Tao W. Novel tumor mutation score versus tumor mutation burden in predicting survival after immunotherapy in pan-cancer patients from the MSK-IMPACT cohort. *Ann Transl Med.* 2020;8(7):446.
9. Doroshow DB, Bhalla S, Beasley MB, Sholl LM, Kerr KM, Gnjatic S, et al. PD-L1 as a biomarker of response to immune-checkpoint inhibitors. *Nat Rev Clin Oncol.* 2021;18(6):345–62.
10. Hanahan D, Weinberg RA. Hallmarks of cancer: the next generation. *Cell.* 2011;144(5):646–74.
11. Lin H, Wei S, Hurt EM, Green MD, Zhao L, Vatan L, et al. Host expression of PD-L1 determines efficacy of PD-L1 pathway blockade-mediated tumor regression. *J Clin Invest.* 2018; 128(2):805–15.
12. Schalper KA, Brown J, Carvajal-Hausdorf D, McLaughlin J, Velcheti V, Syrigos KN, et al. Objective measurement and clinical significance of TILs in non-small cell lung cancer. *J Natl Cancer Inst.* 2015;107(3):dju435. <https://academic.oup.com/jnci/article/107/3/dju435/914032?login=true>
13. Gettinger SN, Choi J, Mani N, Sanmamed MF, Datar I, Sowell R, et al. A dormant TIL phenotype defines non-small cell lung carcinomas sensitive to immune checkpoint blockers. *Nat Commun.* 2018;9(1):3196.
14. Taube JM, Galon J, Sholl LM, Rodig SJ, Cottrell TR, Giraldo NA, et al. Implications of the tumor immune microenvironment for staging and therapeutics. *Mod Pathol.* 2018; 31(2):214–34.
15. Zhang L, Chen Y, Wang H, Xu Z, Wang Y, Li S, et al. Massive PD-L1 and CD8 double positive TILs characterize an immunosuppressive microenvironment with high mutational burden in lung cancer. *J Immunother Cancer.* 2021;9(6):e002356.
16. Liu Y, Zugazagoitia J, Ahmed FS, Henick BS, Gettinger SN, Herbst RS, et al. Immune cell PD-L1 Colocalizes with macrophages and is associated with outcome in PD-1 pathway blockade therapy. *Clin Cancer Res.* 2020;26(4):970–7.
17. Ahmed FS, Gaule P, McGuire J, Patel K, Blenman K, Pusztai L, et al. PD-L1 protein expression on both tumor cells and macrophages are associated with response to neoadjuvant durvalumab with chemotherapy in triple-negative breast cancer. *Clin Cancer Res.* 2020;26(20):5456–61.
18. Peng Q, Qiu X, Zhang Z, Zhang S, Zhang Y, Liang Y, et al. PD-L1 on dendritic cells attenuates T cell activation and regulates response to immune checkpoint blockade. *Nat Commun.* 2020;11(1):4835.
19. Greenwald NF, Miller G, Moen E, Kong A, Kagel A, Dougherty T, et al. Whole-cell segmentation of tissue images with human-level performance using large-scale data annotation and deep learning. *Nat Biotechnol.* 2022;40(4):555–65.
20. Bannon D, Moen E, Schwartz M, Borba E, Kudo T, Greenwald N, et al. DeepCell kiosk: scaling deep learning-enabled cellular image analysis with Kubernetes. *Nat Methods.* 2021;18(1):43–5.
21. Goltsev Y, Samusik N, Kennedy-Darling J, Bhate S, Hale M, Vazquez G, et al. Deep profiling of mouse splenic architecture with CODEX multiplexed imaging. *Cell.* 2018;174(4):968–981.e15.
22. Schürch CM, Bhate SS, Barlow GL, Phillips DJ, Noti L, Zlobec I, et al. Coordinated cellular neighborhoods orchestrate Antitumoral immunity at the colorectal cancer invasive front. *Cell.* 2020;183(3):838.
23. Black S, Phillips D, Hickey JW, Kennedy-Darling J, Venkataraman VG, Samusik N, et al. CODEX multiplexed tissue imaging with DNA-conjugated antibodies. *Nat Protoc.* 2021;16(8):3802–35.
24. Molania R, Gagnon-Bartsch JA, Dobrovic A, Speed TP. A new normalization for Nanostring nCounter gene expression data. *Nucleic Acids Res.* 2019;47(12):6073–83.
25. Risso D, Ngai J, Speed TP, Dudoit S. Normalization of RNA-seq data using factor analysis of control genes or samples. *Nat Biotechnol.* 2014;32(9):896–902.
26. Love MI, Huber W, Anders S. Moderated estimation of fold change and dispersion for RNA-seq data with DESeq2. *Genome Biol.* 2014;15(12):550.
27. Ritchie ME, Phipson B, Wu D, Hu Y, Law CW, Shi W, et al. Limma powers differential expression analyses for RNA-sequencing and microarray studies. *Nucleic Acids Res.* 2015; 43(7):e47.
28. Rohart F, Gautier B, Singh A, Lê Cao KA. mixOmics: an R package for ‘omics feature selection and multiple data integration. *PLoS Comput Biol.* 2017;13(11):e1005752.
29. RStudio Team. RStudio: integrated development for R. RStudio. Boston, MA: PBC; 2020.
30. Therneau, T. A package for survival analysis in R. R package version 3.5-5, 2021. <https://CRAN.R-project.org/package=survival>
31. Wickham H. ggplot2: elegant graphics for data analysis. New York: Springer-Verlag; 2016.
32. Hansen AR, Siu LL. PD-L1 testing in cancer: challenges in companion diagnostic development. *JAMA Oncol.* 2016;2(1): 15–6.
33. Taube JM, Roman K, Engle EL, Wang C, Ballesteros-Merino C, Jensen SM, et al. Multi-institutional TSA-amplified multiplexed immunofluorescence reproducibility evaluation (MITRE) study. *J Immunother Cancer.* 2021;9(7):e002197.
34. Bhattacharya A et al. An approach for normalization and quality control for NanoString RNA expression data. *Brief Bioinform.* 2020;22(3):bbaa163.
35. McGranahan N, Rosenthal R, Hiley CT, Rowan AJ, Watkins TBK, Wilson GA, et al. Allele-specific HLA loss and immune escape in lung cancer evolution. *Cell.* 2017;171(6): 1259–1271.e11.
36. Gettinger S, Choi J, Hastings K, Truini A, Datar I, Sowell R, et al. Impaired HLA class I antigen processing and presentation as a mechanism of acquired resistance to immune checkpoint inhibitors in lung cancer. *Cancer Discov.* 2017;7(12):1420–35.
37. Kim N, Kim HK, Lee K, Hong Y, Cho JH, Choi JW, et al. Single-cell RNA sequencing demonstrates the molecular and cellular reprogramming of metastatic lung adenocarcinoma. *Nat Commun.* 2020;11(1):2285.
38. Goswami KK, Bose A, Baral R. Macrophages in tumor: an inflammatory perspective. *Clin Immunol.* 2021;232:108875.
39. Kamada T, Togashi Y, Tay C, Ha D, Sasaki A, Nakamura Y, et al. PD-1^{hi} regulatory T cells amplified by PD-1 blockade promote hyperprogression of cancer. *Proc Natl Acad Sci.* 2019;116(20):9999–10008.
40. Lowther DE, Goods BA, Lucca LE, Lerner BA, Raddassi K, van Dijk D, et al. PD-1 marks dysfunctional regulatory T cells in malignant gliomas. *JCI Insight.* 2019;1(5):e85935.

41. Peranzoni E, Lemoine J, Vimeux L, Feuillet V, Barrin S, Kantari-Mimoun C, et al. Macrophages impede CD8 T cells from reaching tumor cells and limit the efficacy of anti-PD-1 treatment. *Proc Natl Acad Sci*. 2018;115(17):E4041–50.
42. Smith C, Chang MY, Parker KH, Beury DW, DuHadaway JB, Flick HE, et al. IDO is a nodal pathogenic driver of lung cancer and metastasis development. *Cancer Discov*. 2012;2(8):722–35.
43. Munn DH, Mellor AL. Indoleamine 2,3 dioxygenase and metabolic control of immune responses. *Trends Immunol*. 2013;34(3):137–43.
44. Peggs KS, Quezada SA, Allison JP. Cell intrinsic mechanisms of T-cell inhibition and application to cancer therapy. *Immunol Rev*. 2008;224:141–65.
45. Larkin J, Chiarion-Sileni V, Gonzalez R, Grob JJ, Cowey CL, Lao CD, et al. Combined Nivolumab and Ipilimumab or monotherapy in untreated melanoma. *N Engl J Med*. 2015;373(1):23–34.
46. Mukherjee S, Richardson AM, Rodriguez-Canales J, Ylaya K, Erickson HS, Player A, et al. Identification of EpCAM as a molecular target of prostate cancer stroma. *Am J Pathol*. 2009;175(6):2277–87.
47. Hu B, Ma Y, Yang Y, Zhang L, Han H, Chen J. CD44 promotes cell proliferation in non-small cell lung cancer. *Oncol Lett*. 2018;15(4):5627–33.
48. Kong T, Ahn R, Yang K, Zhu X, Fu Z, Morin G, et al. CD44 promotes PD-L1 expression and its tumor-intrinsic function in breast and lung cancers. *Cancer Res*. 2020;80(3):444–57.
49. Moutafi MK, Molero M, Martinez Morilla S, Baena J, Vathiotis IA, Gavrieliatou N, et al. Spatially resolved proteomic profiling identifies tumor cell CD44 as a biomarker associated with sensitivity to PD-1 axis blockade in advanced non-small-cell lung cancer. *J Immunother Cancer*. 2022;10(8):e004757.
50. West EE, Jin HT, Rasheed AU, Penaloza-MacMaster P, Ha SJ, Tan WG, et al. PD-L1 blockade synergizes with IL-2 therapy in reinvigorating exhausted T cells. *J Clin Invest*. 2013;123(6):2604–15.
51. Schwartzenuber DJ, Lawson DH, Richards JM, Conry RM, Miller DM, Treisman J, et al. gp100 peptide vaccine and interleukin-2 in patients with advanced melanoma. *N Engl J Med*. 2011;364(22):2119–27.
52. Rosenberg SA. IL-2: the first effective immunotherapy for human cancer. *J Immunol*. 2014;192(12):5451–8.
53. Hsu EJ, Cao X, Moon B, Bae J, Sun Z, Liu Z, et al. A cytokine receptor-masked IL2 prodrug selectively activates tumor-infiltrating lymphocytes for potent antitumor therapy. *Nat Commun*. 2021;12(1):2768.
54. Sun Z, Ren Z, Yang K, Liu Z, Cao S, Deng S, et al. A next-generation tumor-targeting IL-2 preferentially promotes tumor-infiltrating CD8+ T-cell response and effective tumor control. *Nat Commun*. 2019;10(1):3874.
55. Klement JD, Paschall AV, Redd PS, Ibrahim ML, Lu C, Yang D, et al. An osteopontin/CD44 immune checkpoint controls CD8+ T cell activation and tumor immune evasion. *J Clin Invest*. 2018;128(12):5549–60.
56. Zheng Y, Hao S, Xiang C, Han Y, Shang Y, Zhen Q, et al. The correlation between SPP1 and immune escape of EGFR mutant lung adenocarcinoma was explored by bioinformatics analysis. *Front Oncol*. 2021;11:592854.
57. Liu Y, Xun Z, Ma K, Liang S, Li X, Zhou S, et al. Identification of a tumour immune barrier in the HCC microenvironment that determines the efficacy of immunotherapy. *J Hepatol*. 2023;78:770–82.
58. Clemente N et al. Osteopontin bridging innate and adaptive immunity in autoimmune diseases. *J Immunol Res*. 2016;2016:7675437.
59. Overacre-Delgoffe AE, Chikina M, Dadey RE, Yano H, Brunazzi EA, Shayan G, et al. Interferon- γ drives T(reg) fragility to promote anti-tumor immunity. *Cell*. 2017;169(6):1130–1141.e11.
60. Sanmamed MF, Nie X, Desai SS, Villaroel-Espindola F, Badri T, Zhao D, et al. A burned-out CD8(+) T-cell subset expands in the tumor microenvironment and curbs cancer immunotherapy. *Cancer Discov*. 2021;11(7):1700–15.
61. Badovinac VP, Tvinnereim AR, Harty JT. Regulation of antigen-specific CD8⁺ T cell homeostasis by perforin and interferon- γ . *Science*. 2000;290(5495):1354–7.
62. Refaeli Y, van Parijs L, Alexander SI, Abbas AK. Interferon γ is required for activation-induced death of T lymphocytes. *J Exp Med*. 2002;196(7):999–1005.
63. Wherry EJ. T cell exhaustion. *Nat Immunol*. 2011;12(6):492–9.

SUPPORTING INFORMATION

Additional supporting information can be found online in the Supporting Information section at the end of this article.

How to cite this article: Monkman J, Kim H, Mayer A, Mehdi A, Matigian N, Cumberbatch M, et al. Multi-omic and spatial dissection of immunotherapy response groups in non-small cell lung cancer. *Immunology*. 2023. <https://doi.org/10.1111/imm.13646>